Electronic Supplementary Material (ESI) for New Journal of Chemistry.

Supporting Information

Synthesis of A Series of Porous Aromatic Frameworks by Mechanical ball milling.

Xiaolu Chen, Zhenyan Yuan, Yingchun Zhong, Fuxing Sun, Hao Ren*

State Key Laboratory of Inorganic Synthesis and Preparative Chemistry, College of Chemistry, Jilin University, Changchun 130012, China

1 Experimental Section

1.1 Chemicals

P-terphenyl (purity 98%) and o-terphenyl (purity, 98%) were purchased from Shanghai Aladdin Bio-Chem Technology Co., LTD. Anhydrous $FeCl_3$ (purity, 99%); Formaldehyde dimethyl acetal (FDA, purity, 98%) and anhydrous methanol were purchased from Anhui Zesheng Technology Co., LTD (Energy Chemical). Other reagents were purchased from commercial suppliers.

1.2 Synthesis of PAF-104s and PAF-105s

1.2.1 Synthesis of PAF-104a-c and PAF-105a-c

The synthetic process of PAF-104a-c and PAF-105a-c are consistent, and the molar ratio of $FeCl_3$ and p-terphenyl or o-terphenyl is adjusted as 3:1, 6:1 and 12:1, respectively. Taking PAF-104a as an example, the specific procedures are as follows: Firstly, anhydrous $FeCl_3$ (1.056 g, 6.51 mmol) and p-terphenyl (500 mg, 2.17 mmol) with a molar ratio of 3:1 is added into the stainless steel ball grinding tank. Then, the stainless steel ball grinding tank is sealed and tightened and put into the ball mill. After ball grinding 2 h, the product is washed with HCl (1M), H_2O and anhydrous methanol successively. The product is further Soxhlet extracted with anhydrous methanol for 24 h. Finally, the obtained product is dried under vacuum at 120 ℃ for 12 h (440 mg, 88 %).

1.2.2 Synthesis of PAF-104d-g and PAF-105d-g

The synthetic process of PAF-104d-g and PAF-105d-g are consistent, and the molar ratio of $FeCl_3$ and p-terphenyl or o-terphenyl is adjusted as 3:1, 6:1 and 12:1, respectively. Taking PAF-104d as an example, the specific procedures are as follows: Firstly, anhydrous $FeCl_3$ (1.056 g, 6.51 mmol) and p-terphenyl (500 mg, 2.17 mmol) are added into the stainless steel ball grinding tank. Then FDA (0.55 mL, 6.51 mmol) is added, and the molar ratio of $FeCl_3$, FDA and p-terphenyl is 3:3:1. The stainless steel ball grinding tank is sealed and tightened and put into the ball mill. After ball grinding 2 h, the product is washed with HCl (1M), H_2O and anhydrous methanol successively. The product is further Soxhlet extracted with anhydrous methanol for 24 h. The

obtained product was dried under vacuum at 120 ℃ for 12 h (449 mg, 89 %).

1.3 Instruments

Fourier transform infrared (FT-IR) spectra were determined by Bruker VERTEX 80 using the KBr pellet technique. Scanning electron Microscope (SEM) was performed by JEOL Jsm-6700f. Elemental analysis was tested by Vario Micro Cube Elemental Analyzer. Thermal gravimetric analysis (TGA) was carried out on TA Q500 Thermogravimetric Analyzer at the heating rate of 10 ℃ min^{-1} under air condition. X-ray photoelectron spectroscopy (XPS) was performed with Thermo ESCALAB 250 X-ray Photoelectron Spectroscopy. Solid-state ^{13}C CP/MAS NMR measurement was performed on a Bruker Avance Neo 600WB NMR spectrometer. The Nitrogen adsorption isotherms were measured on the Quantachrome Autosorb-iQ_2 analyzer at 77 K. The gas sorption isotherms were measured using Quantachrome Autosorb-iQ_2 adsorption analyzer.

2 Isotherms fitting and IAST calculation of selectivity

The adsorption isotherms in PAF-104f and PAF-105g were fitted using a dual-site Langmuir model:

$$q=\frac{q_1^{max}(b_1p)^{1/n_1}}{1+(b_1p)^{1/n_1}}+\frac{q_2^{max}(b_2p)^{1/n_2}}{1+(b_2p)^{1/n_2}}$$

Here, p is the pressure of the bulk gas at equilibrium with the adsorbed phase (kPa), q is the adsorbed amount per mass of adsorbent (mol kg^{-1}), q_1^{max} and q_2^{max} are the saturation capacities of site A and site B (mol kg^{-1}), b_1 and b_2 are the affinity coefficients of site A and B (kPa^{-1}), n_1 and n_2 represents the deviation from an ideal homogeneous surface.

The IAST adsorption selectivity for two gases is defined as:

$$S=\frac{q_1/q_2}{p_1/p_2}$$

Where q_1 and q_2 are the absolute component loadings of the adsorbed phase in the mixture, and p_1 and p_2 are the component partial pressures.

3 Supplementary Figures

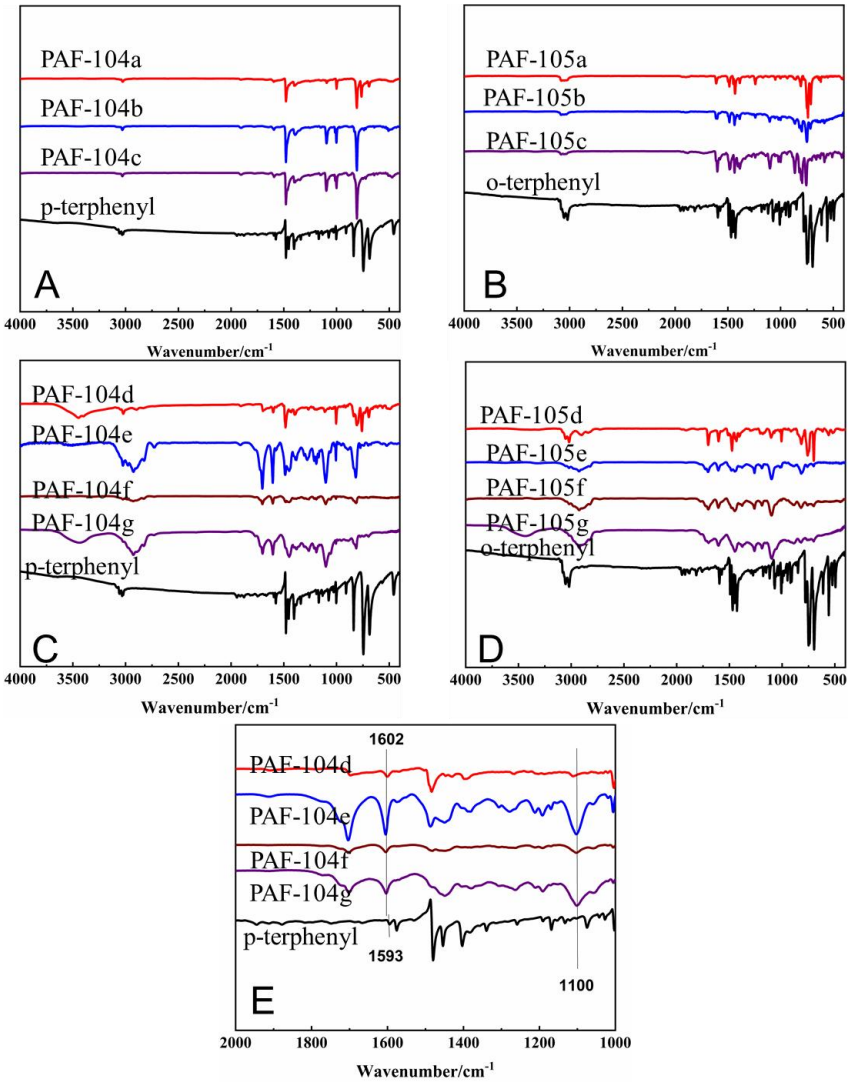

Fig S1 (A, B) FTIR spectra of PAF-104a-c and p-terphenyl, (C, D) FTIR spectra of PAF-104d-g and p-terphenyl, (E) FTIR spectra of PAF-104d-g and p-terpheny.

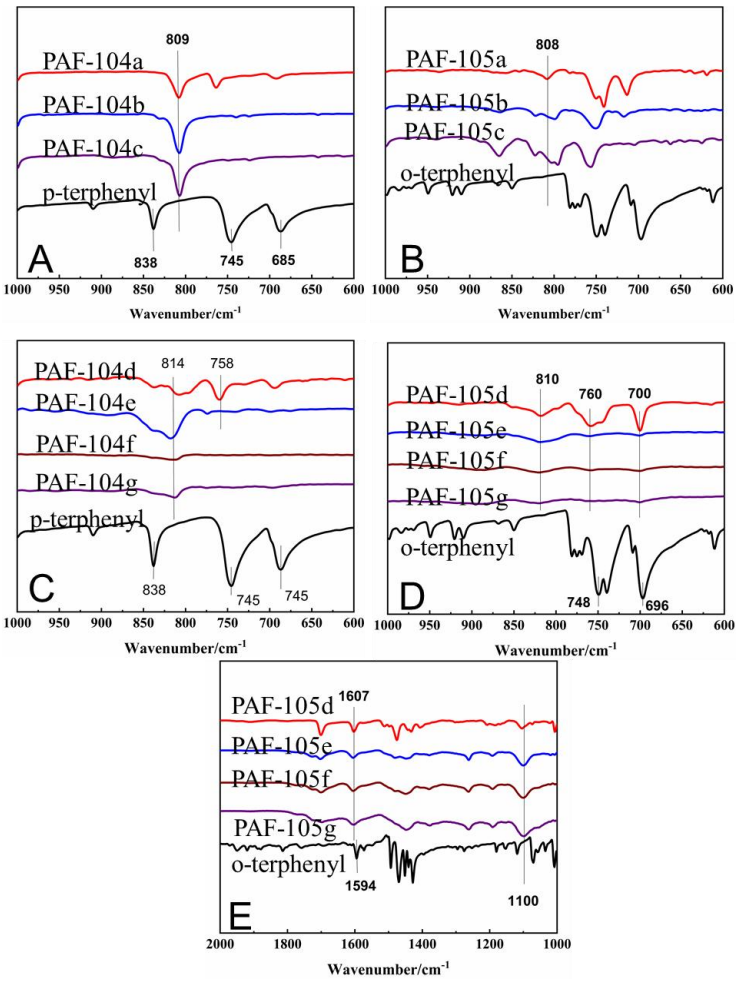

Fig S2 (A, B) FTIR spectra of PAF-105a-c and o-terphenyl, (C, D, E) FTIR spectra of PAF-105d-g and o-terphenyl.

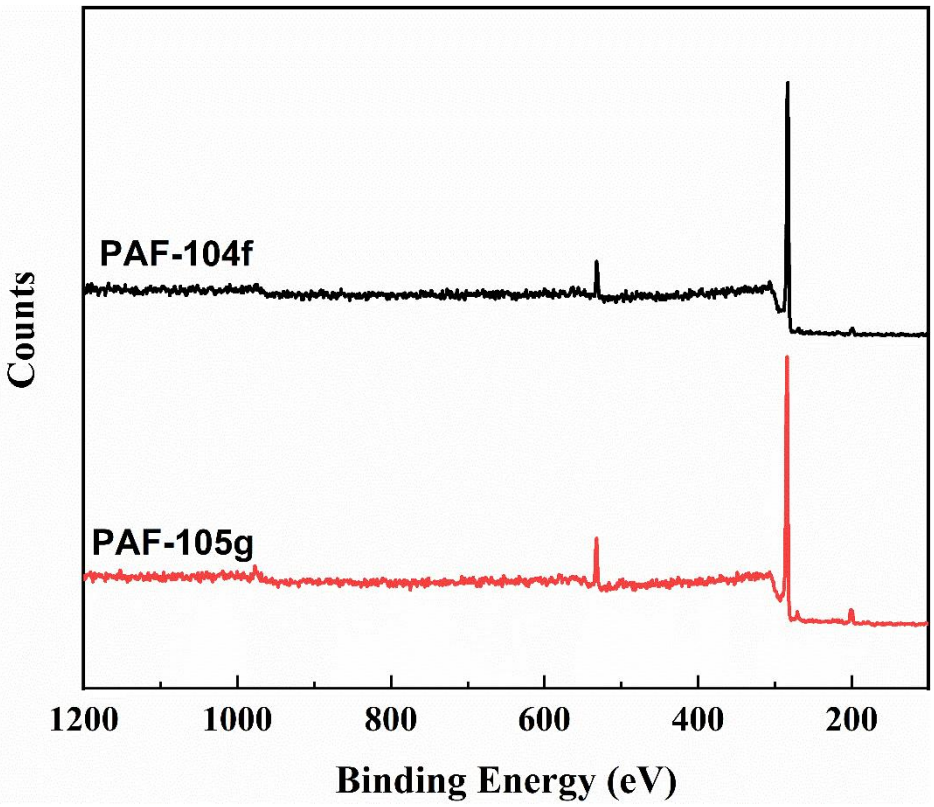

Fig S3 XPS spectra of PAF-104f and PAF-105g.

Table S1 CHON of PAF-104f and PAF-105g.

	C(%)	H(%)	O(%)	C/H
PAF-104f	78.68	4.993	12.644	15.7568
PAF-105g	81.65	4.946	12.033	16.5087

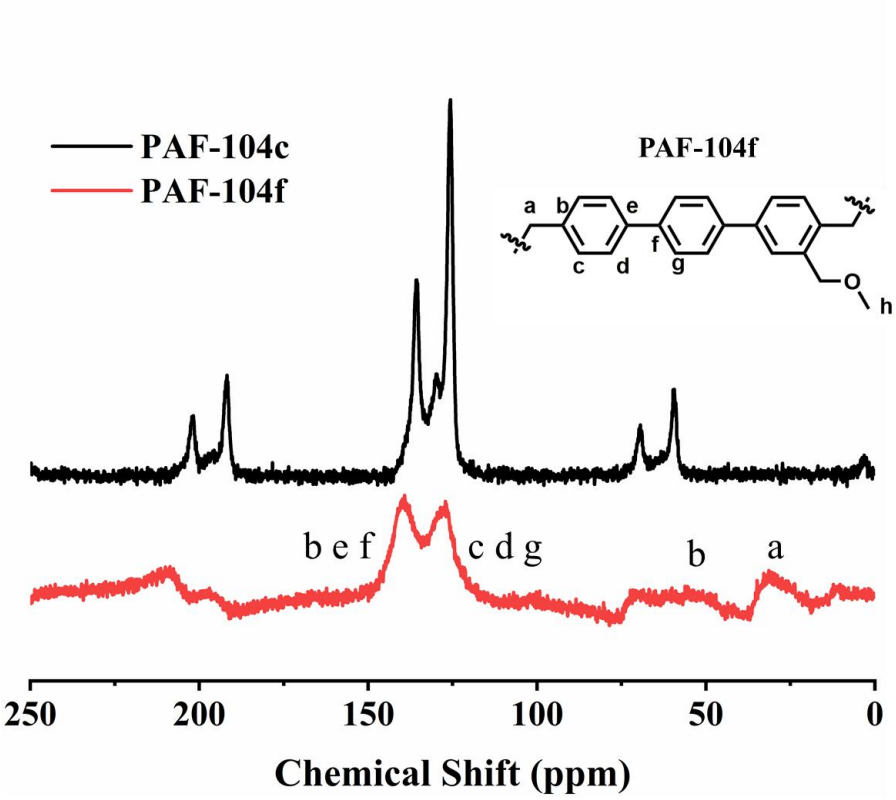

Fig S4 ^{13}C CP/MAS NMR spectra of PAF-104c and PAF-104f.

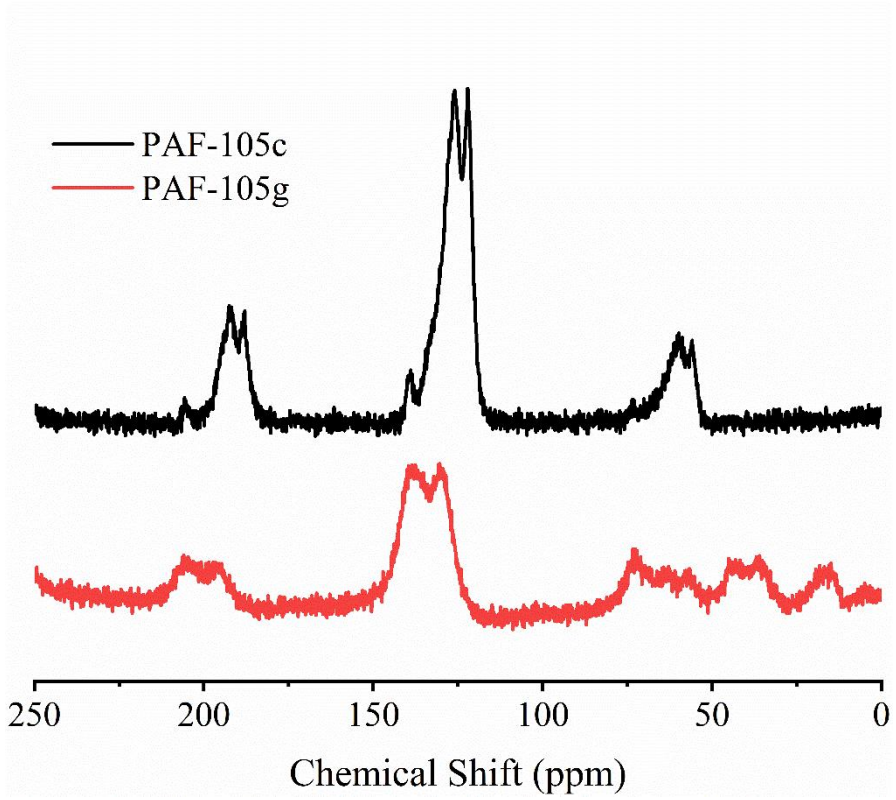

Fig S5 ^{13}C CP/MAS NMR spectra of PAF-105c and PAF-105g.

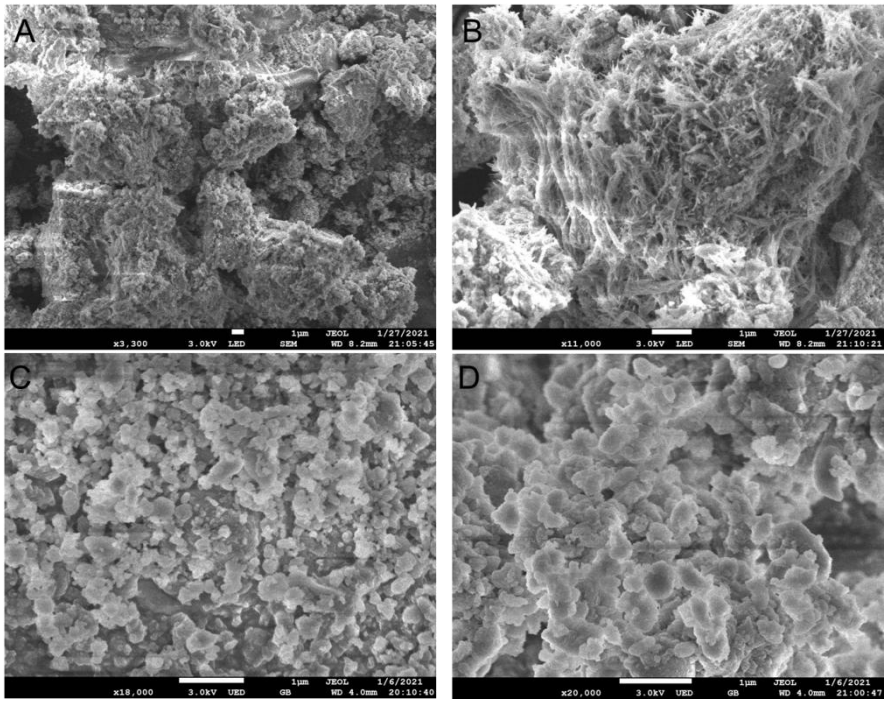

Fig S6 SEM images of PAF-104c (A), PAF-105c (B), PAF-104f (C), and PAF-105g (D).

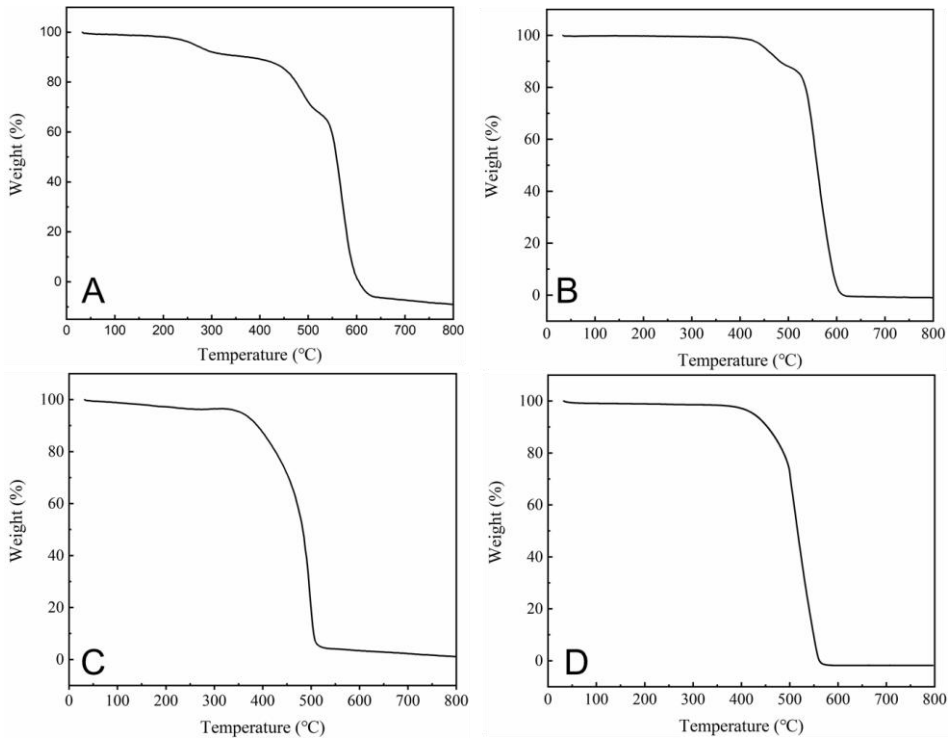

Fig S7 TGA curve of PAF-104c (A), PAF-105c (B), PAF-104f (C), and PAF-105g (D).

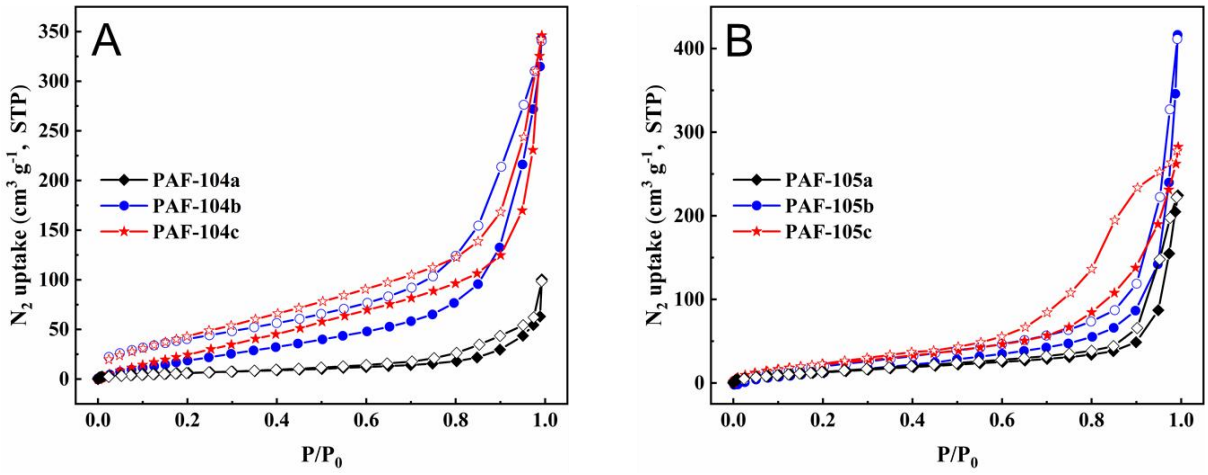

Fig S8 (A) N_2 adsorption-desorption isotherms of PAF-104a-c; (B) N_2 adsorption-desorption isotherms of PAF-105a-c.

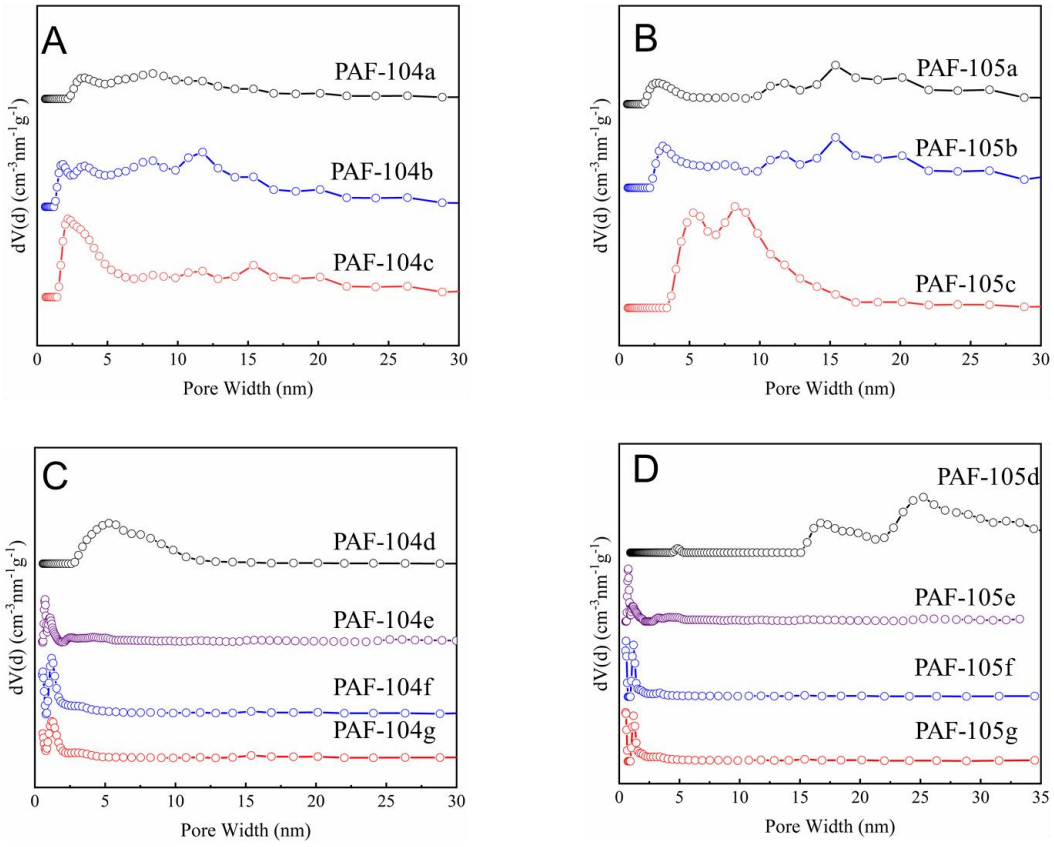

Fig S9 Pore size distribution of PAF-104s (A, C) and PAF-105s (B, D).

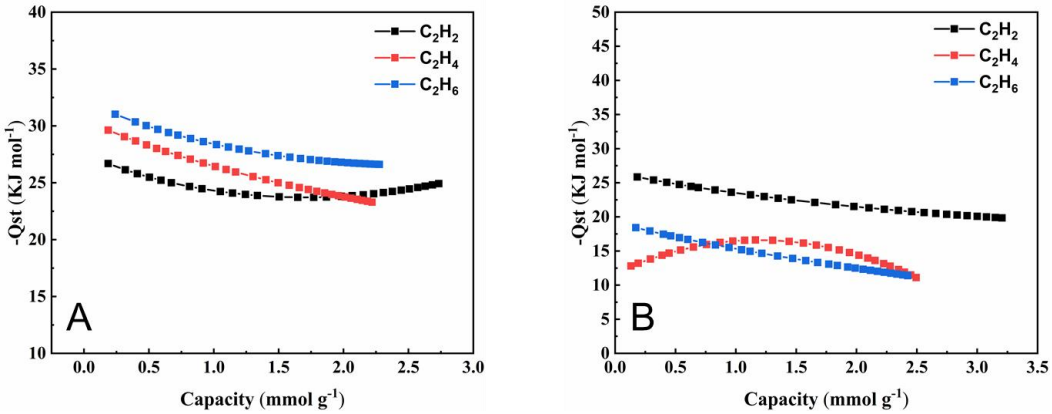

Fig S10 The Qst of C_2H_2, C_2H_4, and C_2H_6 for PAF-104f (A) and PAF-105g (B)

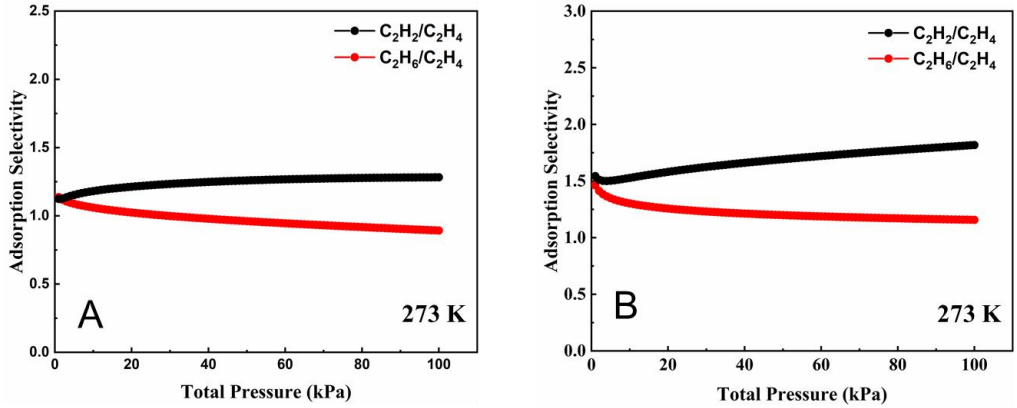

Fig S11 The selectivity of C_2H_2/C_2H_4 and C_2H_6/C_2H_4 for PAF-104f (A) and PAF-105g (B) at 273 K.

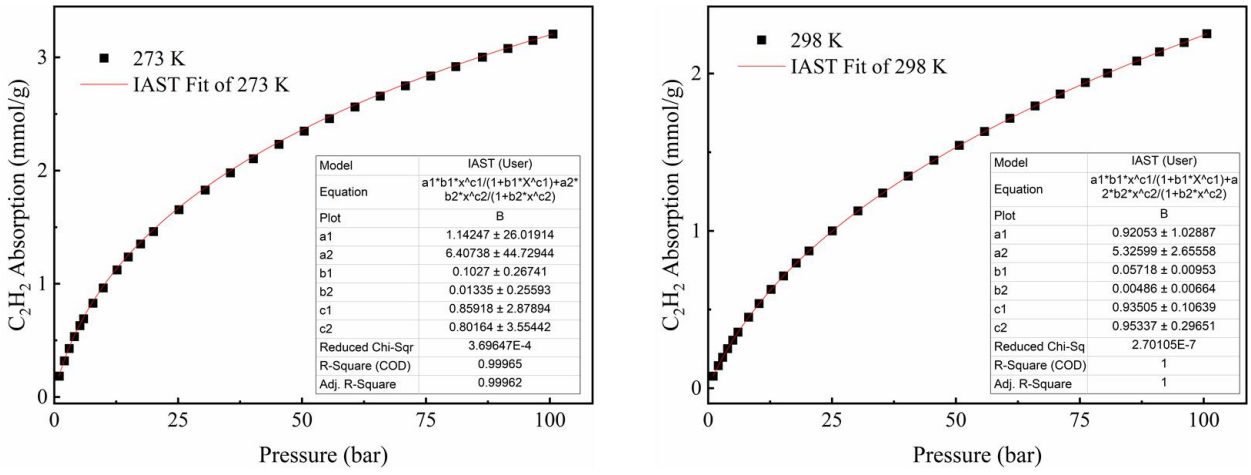

Fig S12 Fitted line plots of C_2H_2 for PAF-104f at 273 K and298 K.

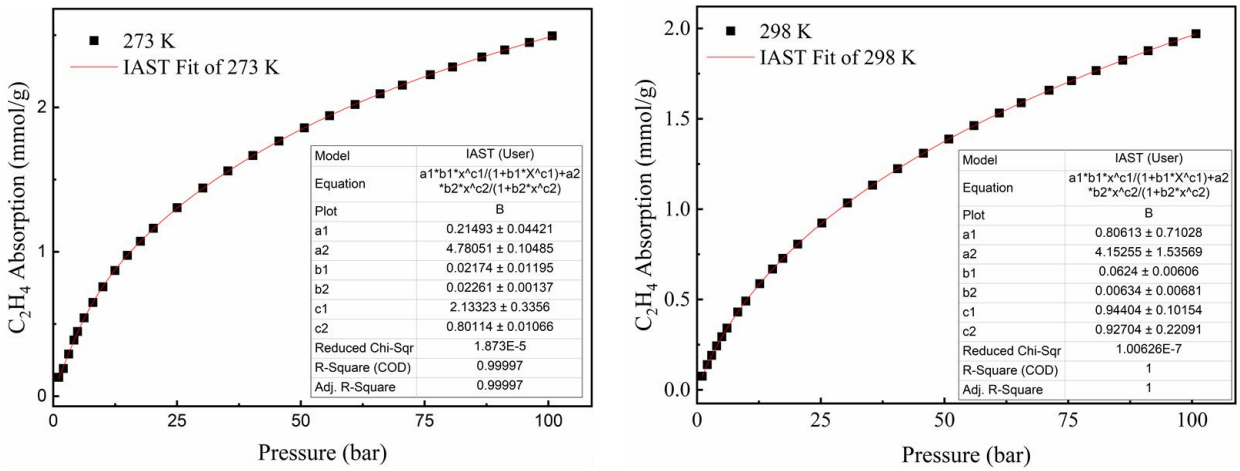

Fig S13 Fitted line plots of C_2H_4 for PAF-104f at 273 K and298 K.

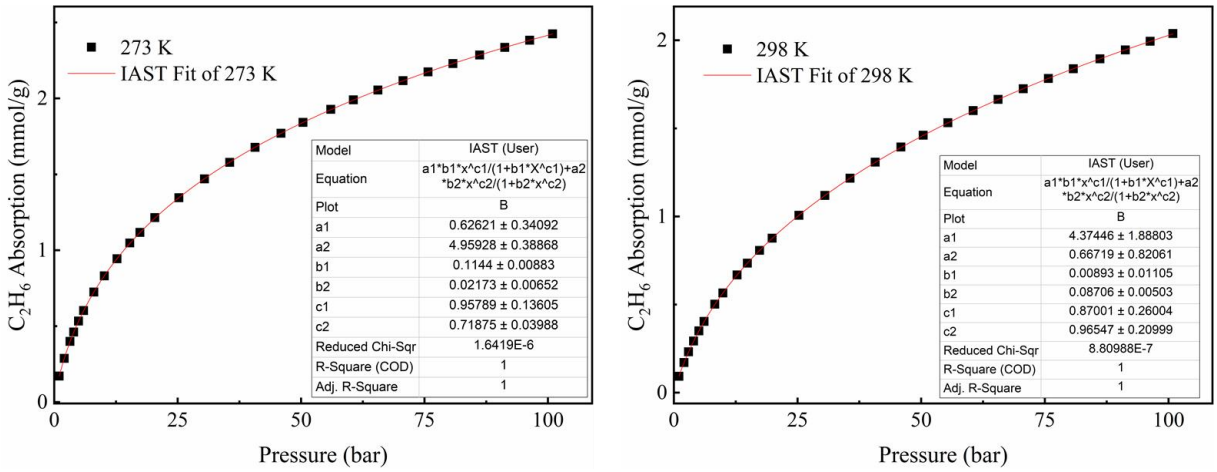

Fig S14 Fitted line plots of C_2H_6 for PAF-104f at 273 K and298 K.

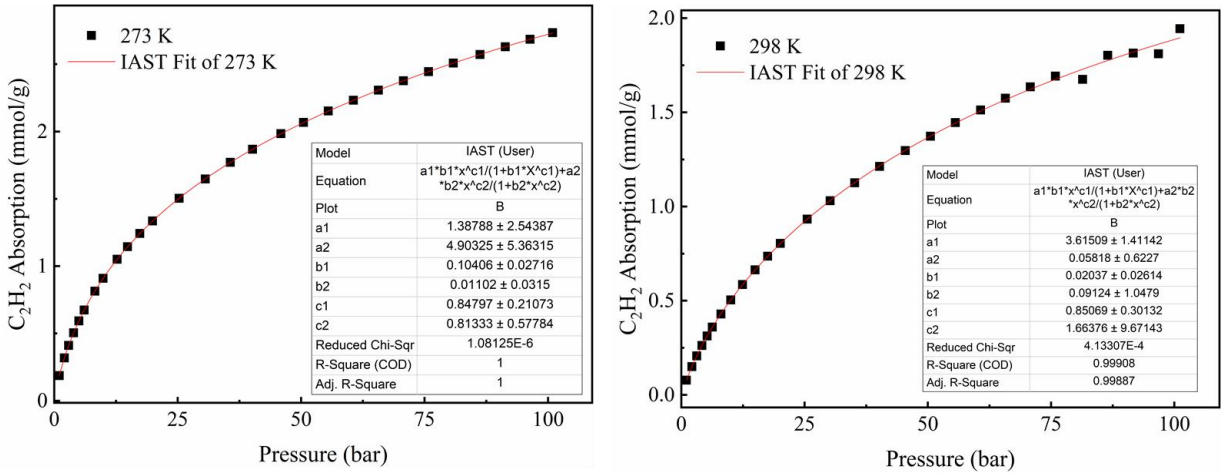

Fig S15 Fitted line plots of C_2H_2 for PAF-105g at 273 K and298 K.

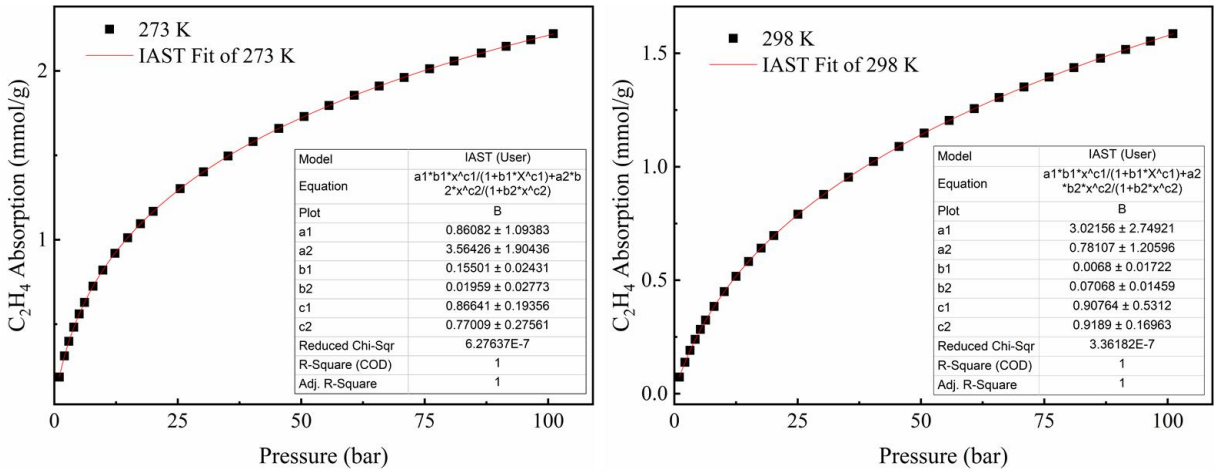

Fig S16 Fitted line plots of C_2H_4 for PAF-105g at 273 K and298 K.

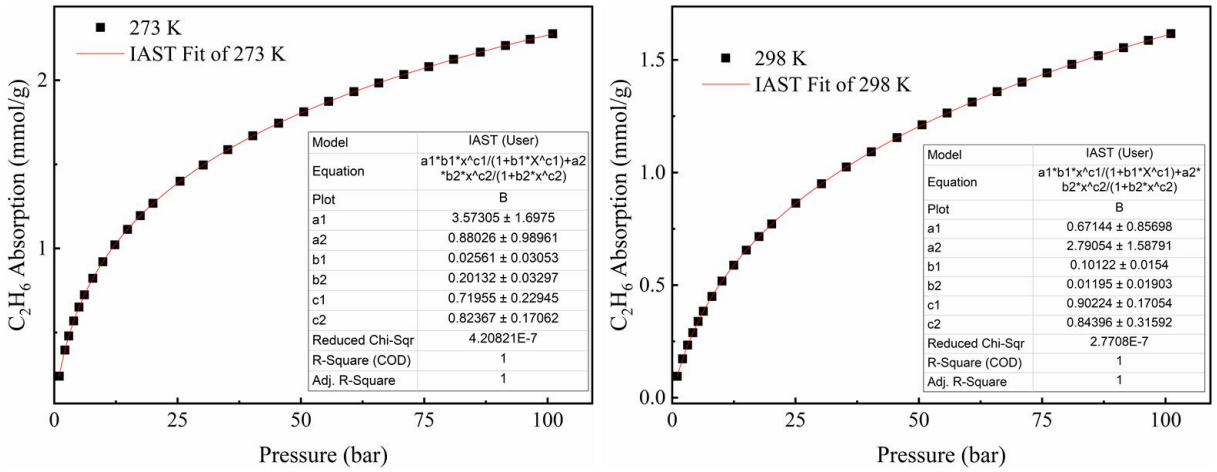

Fig S17 Fitted line plots of C_2H_6 for PAF-105g at 273 K and298 K.

Table S2 Dual-site Langmuir fitting parameters of PAF-104f for C_2H_2, C_2H_4, and C_2H_6 at 273 K and 298 K.

273 K	Site A			Site B			R^2
	$q_{1,}^{max}$	b_1	$1/n_1$	$q_{2,}^{max}$	b_2	$1/n_2$	
C_2H_2	1.14	0.10	0.86	6.41	0.01	0.80	0.9996
C_2H_4	0.21	0.021	2.13	4.78	0.022	0.80	0.9999
C_2H_6	0.63	0.11	0.95	4.95	0.02	0.72	1
298 K	Site A			Site B			
	$q_{1,}^{max}$	b_1	$1/n_1$	$q_{2,}^{max}$	b_2	$1/n_2$	R^2
C_2H_2	0.92	0.06	0.93	5.32	5E-5	0.94	0.9999
C_2H_4	0.81	0.06	0.94	4.15	0.006	0.93	1
C_2H_6	4.37	0.01	0.87	0.66	0.08	0.96	1

Table S3 Dual-site Langmuir fitting parameters of PAF-105g for C_2H_2, C_2H_4, and C_2H_6 at 273 K and 298 K.

273 K	Site A			Site B			R^2
	$q_{1,}^{max}$	b_1	$1/n_1$	$q_{2,}^{max}$	b_2	$1/n_2$	
C_2H_2	1.39	0.10	0.85	4.90	0.01	0.81	1
C_2H_4	0.86	0.15	0.86	3.56	0.02	0.77	1
C_2H_6	3.57	0.026	0.72	0.88	0.20	0.82	1
298 K	Site A			Site B			
	$q_{1,}^{max}$	b_1	$1/n_1$	$q_{2,}^{max}$	b_2	$1/n_2$	R^2
C_2H_2	3.61	0.02	0.85	0.058	0.09	1.66	0.99908
C_2H_4	3.02	0.007	0.91	0.78	0.07	0.92	0.9999
C_2H_6	0.67	0.10	0.90	2.80	0.012	0.84	1

Table S4 The summary of C_2H_2 adsorption of some porous materials.

No.	materials	C_2H_2		Ref
		273 K	298 K	
1	SOF-1a	61	50	[1]
2	HOF-1a	63	57	[1]
3	HOF-3a	58	47	[1]
4	HOF-5a	183	182	[1]
5	HOF-BTB	110.3	64.3	[1]
6	iPAF-1-OH	150	101.1	[2]
7	iPAF-1-F	112	87.5	[2]
8	iPAF-1-Cl	68	46.3	[2]
9	CPOCC-101α		95	[3]
10	P(Ph-3MVIm-Cl)	43.5	32.7	[4]
11	P(Ph-3MVIm-SiF_6)	39.5	29.5	[4]
12	P(Ph-6MVIm-Br)	43	33.5	[4]
13	PAF-110	77.9	49.9	[5]
14	PAF-106c	11.5	10.3	[6]
15	CTF-PO71	104	74	[7]
16	PAF-104f	71.8	55.9	This work
17	PAF-105g	61.2	38.3	This work

Table S5 The summary of C_2H_6/C_2H_4 selectivity of some porous materials.

No.	materials	T/K	P/bar	S(C_2H_6/C_2H_4)	Ref
1	COF-1	298	1	1.92	[8]
2	COF-6	298	1	1.18	[8]
3	COF-8	298	1	1.20	[8]
4	COF-10	298	1	1.15	[8]
5	MCOF-1	298	1	1.75	[8]
6	COF-102	298	1	1.48	[8]
7	COF-300	298	1	1.59	[8]
8	COF-320	298	1	1.50	[8]
9	Ni-DBA-3D-COF	295	1	1.15	[8]
10	CTF-DCTC-400	298	1	1.04	[9]
11	CTF-DCTC-500	298	1	2.08	[9]
12	ZIF-7	298	1	1.02	[10]
13	PAF-106c	298	1	1.08	[6]
14	HIAM-112	298	1	1.9	[11]
15	PAF-104f	298	1	1.24	This work
16	PAF-105g	298	1	1.20	This work

Reference

[1] T. U. Yoon, S. B. Baek, D. W. Kim, E. J. Kim, W. J. Lee, B. K. Singh, M. S. Lah, Y. S. Bae and K. S. Kim, *Chem. Commun*., 2018, **54**, 9360-9363.

[2] P. P. Zhang, X. Q. Zou, J. Song, Y. Y, Tian, Y. L. Zhu, G. L. Yu, Y. Yuan and G. S. Zhu, *Adv. Mater.*, 2020, **32**, 1907449.

[3]W. J. Wang, K. Z. Su, E. S. M. EI-Sayed, M. Yang and D. Q. Yuan, *ACS App. Mater. Inter.,* 2021, **13**, 24042−24050.

[4]X. Suo, X. L. Cui, L. F. Yang, N. Xu, Y. Q. Huang, Y. He, S. Dai and H. B. Xing, *Adv. Mater.,* 2020, **32**, 1907601.

[5]L. C. Jiang, Y. Y. Tian, T. Sun, Y. L. Zhu, H. Ren, X. Q. Zou, Y. H. Ma, K. R. Meihaus, J. R. Long and G. S. Zhu, J. Am. Chem. Soc., 2018, 140, 15724-15730.

[6]X. L. Chen, Z. Y. Yuan, Y. C. Zhong and H. Ren, *Chem. J. Chin. Univ.*, 2022, **43**, 20210771.

[7]Y. Lu, J. He, Y. L. Chen, H. Wang, Y. F. Zhao and Y. Ding, *Macromol. Rapid Commun.,* 2017, **39**, 1700468.

[8]C. He, Y. Wang, Y. Chen, X. Wang, J. Yang, L. Li and J. Li, *ACS App. Mater. Inter.*, 2020, **12**, 52819-52825.

[9]Y. J. Chang, H. L. Huang, H. J. Zhu, Y. L. Zhao, L. Wang, Y. X. Sun and C. L. Zhong, *Chem. Eng. J.,* 2022, **427**, 131726.

[10]H. Thakkar, Q. Al-Naddaf, N. Legion, M. Hovis, A. Krishnamurthy, A. A. Rownaghi and F. Rezaei, *ACS Sustain. Chem. Eng.,* 2018, **6**, 15228-15237.

[11]J. Q. Liu, J. F. Miao, S. Ullah, K. Zhou, L. Yu, H. Wang, Y. F. Wang, T. Thonhauser and J. Li, *ACS. Mater. Lett.*, 2022, **4**, 1227-1232.